Ionospheric ion and electron heating at the poleward boundary of a poleward expanding substorm-disturbed region

JOURNAL OF GEOPHYSICAL RESEARCH, VOL. 106, NO. A7, PAGES 12,845–12,862, JULY 1, 2001

Ionospheric ion and electron heating at the poleward boundary of a poleward expanding substorm-disturbed region

N. J. Fox,[1,2] S. W. H. Cowley,[3] J. A. Davies,[3] R. A. Greenwald,[1]
M. Lester,[3] M. Lockwood,[4] and H. Lühr[5]

Abstract. We present observations of a poleward propagating substorm-disturbed region which was observed by the European Incoherent SCATter (EISCAT) radar and the Svalbard International Monitor for Auroral Geomagnetic Effects (IMAGE) magnetometers in the post-midnight sector. The expansion of the disturbance was launched by a substorm intensification which started ~25 min after the initial onset, and ~10 min before the disturbance arrived over Svalbard. In association with the magnetic disturbance, a poleward expanding enduring enhancement in the *F* region electron temperature was observed, indicative of soft electron precipitation, with a narrow band of enhanced ion temperature straddling its poleward edge, indicative of fast ion flows and ion-neutral collisional heating. This electron temperature boundary was coincident with the poleward propagating electrojet current system detected by the high-latitude IMAGE magnetometer stations and is taken to be a proxy for the observation of a substorm auroral bulge. The electron temperature boundary is inferred to have a width comparable or less than one radar range gate (~60 km transverse to the magnetic field), while the region of high ion temperature was found to be approximately three gates wide, extending approximately two gates (~120 km) poleward of the electron temperature boundary, and approximately one gate (~60 km) equatorward. The two-beam radar line-of-sight velocity data are found to be consistent with the existence of a layer of high-speed flow in the boundary, peaking at values ~1.5-3 km s^{-1}, roughly consistent with the ion temperature data. The flow is directed either east or west along the boundary depending on the direction of the flow in the poleward region. We infer that the flow is deflected along and around the boundary of the substorm-disturbed region due to the high conductivity of the latter. Variations in the flow poleward of the boundary produced no discernible magnetic effects on the ground, confirming the low conductivity of the preboundary ionosphere.

1. Introduction

In the high-latitude ionosphere the growth phase of a substorm is characterized by the presence of equatorward drifting discrete auroral arcs in the nightside hours, together with growing magnetic disturbances associated with the twin-vortical *DP* 2 current system [*Pellinen and Heikkila*, 1984]. At the onset of the expansion phase the most equatorward of these arcs suddenly brightens in a restricted local time sector near magnetic midnight, forming an auroral bulge which expands poleward and toward dusk and dawn at speeds of about 1–2 km s^{-1} [*Akasofu*, 1964]. In this bulge the substorm westward electrojet current flows, connecting the ionosphere to a dipolarized region of the tail via the substorm-wedge current system [*McPherron et al.*, 1973]. *Persson et al.* [1994a, b] used European Incoherent SCATter (EISCAT) radar data in a southward pointing beam configuration to study the auroral bulge shortly after onset, and found that it was associated with a poleward propagating electron temperature enhancement in the *F* region ionosphere, which is due to electron precipitation. They also found an ion temperature enhancement to be present in the region of its poleward border. Subsequently, the bulge continues to expand over an interval typically of 10–20 min, extending to cover an area of ~10° in latitude, and several hours of local time on either side of midnight. *Fukunishi et al.* [1993], using data from the Akebono spacecraft, found a field-aligned current system which they termed "Region 0" (R0) at the poleward edge of the bulge, which is opposite in sense to the Region 1/substorm wedge field-aligned currents (R1) flowing in the immediately equatorward region. *Fujii et al.* [1994] subsequently found, using Dynamics Explorer 2 spacecraft data, that the R0 current and the poleward part of the R1 current are associated with the occurrence of "spike-like" electric field structures. Within these structures the north-south electric field was found to peak at ~50 mV m^{-1}, typically a factor of 2 or 3 times the field strength observed in the regions immediately poleward and equatorward. The corresponding plasma flow speed is ~1 km s^{-1}, with the flow directed eastward within the local time sector of the bulge and duskward thereof, and westward at local times dawnward of the bulge. The latitudinal width of the "spike-like" electric fields was found to be ~50–100 km (i.e., 0.5°–1° of magnetic latitude), located typi-

[1]Applied Physics Laboratory, Johns Hopkins University, Laurel, Maryland.
[2]Laboratory for Extraterrestrial Physics, NASA Goddard Space Flight Center, Greenbelt, Maryland.
[3]Department of Physics and Astronomy, University of Leicester, Leicester, England.
[4]Rutherford Appleton Laboratory, Oxfordshire, England.
[5]GeoForschungsZentrum Potsdam, Potsdam, Germany.

Paper number 1999JA000387.
0148-0227/01/1999JA000387$09.00

cally poleward of, or straddling, the poleward boundary of intense auroral electron precipitation.

In this paper we study high time resolution observations made by the EISCAT VHF radar during an interval in which a substorm-disturbed region propagated poleward along the radar beams. These observations reveal that a layer of enhanced F region ion temperature, ~180 km thick, straddled the boundary of the substorm-disturbed region as it propagated poleward. We discuss the origins of this layer and conclude that it is due to a corresponding layer of elevated plasma flows, ~1–2 km s^{-1}, and resulting ion-neutral frictional heating. These features appear to represent the radar counterpart of the "spike-like" electric field regions found in spacecraft data by *Fujii et al.* [1994].

2. Interval Overview

We discuss an interval of substorm disturbance observed on December 7, 1992, by ground-based radars and magnetometers. A full discussion of the geophysical context of this data set is given by *Fox et al.* [1999], including a description of the instruments used to collect the data. Here we concentrate on observations of a poleward propagating substorm-disturbed region by the EISCAT VHF radar and magnetometers of the International Monitor for Auroral Geomagnetic Effects (IMAGE) chain. Figure 1 shows the locations of the magnetometer stations whose data are employed in this study (open circles) together with the location of the radar transmitter site at Tromsø (solid circle). The lines drawn from the latter show the directions of the two radar beams employed, as will be discussed further below.

We first examine data from the IMAGE magnetometer chain in order to provide a context for the EISCAT radar observations. Figure 2 presents the X (geographic northward) and Z (vertically downward) components of the magnetic field (from which the daily mean has been subtracted yielding the dotted zero lines) for the interval 2200–2400 UT. This interval corresponds to the midnight and early postmidnight sectors, since magnetic local time (MLT) ≈ UT + 2.5 hours on the IMAGE meridian. Following an interval of southward interplanetary magnetic field (as determined from Galileo data [not shown] in the tail magnetosheath during the second Earth encounter), the onset of a substorm expansion phase took place at ~2215 UT. An onset of activity in the Pi2 wave band also took place simultaneously as observed by the Sub-Auroral Magnetometer Network (SAMNET) magnetometer chain, while an energetic particle injection was detected by the Los Alamos National Laboratory (LANL) geosynchronous satellites at ~2218 UT [see *Fox et al.*, 1999]. At onset the westward electrojet was centered just poleward of station PEL (62.4°N magnetic latitude), as indicated by both the maximum negative perturbation in the X component at that station, and the reversal in the Z component perturbation from positive to its north, to negative to its south. After intensifying over an interval of ~15 min, this initial disturbance started to recover but was then followed by a second intensification starting at ~2240 UT centered around station MAS (64.9°N), which was associated with an enhancement of activity in the Pi2 wave band observed by the SAMNET, together with further particle injections detected by the LANL spacecraft. After this time the substorm-disturbed region expanded rapidly poleward, reaching the Svalbard magnetometers BJO, HOP, HOR, and NAL after ~2250 UT. Thus the disturbance moved poleward at a speed of ~1 km s^{-1}. Spike-like minima in the X component were observed at BJO

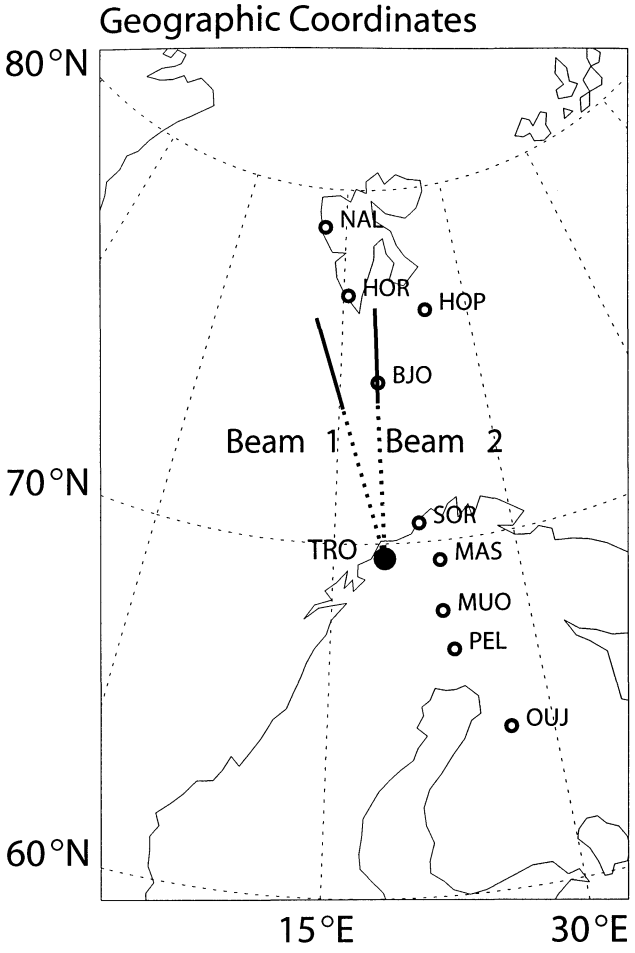

Figure 1. Map in geographic coordinates showing the relative locations of the magnetometer stations of the IMAGE chain, shown by the open circles, and the two beams formed by the EISCAT VHF radar, shown by the dashed and solid lines. The solid portions of these lines show the ranges over which the radar beams pass through the F region ionosphere from which useful returned signal is obtained (gates 1–7). The solid circle represents the location of the radar transmitter site at Tromsø.

(70.1°N), HOP (71.4°N), and HOR (72.8°N) at ~2250 and ~2300 UT. After ~2250 UT, however, the bays in the central part of the active region (MUO, MAS, and SOR) started to recover, while those poleward and equatorward intensified, leading to a "double electrojet" configuration after ~2300 UT. The double structure was seen both in the latitudinal variation in the magnitude of the X component, and in the multiple reversals in the polarity of the Z component with latitude. Thus two separate current systems were present during the later interval. The lower latitude (main) substorm current was again centered near PEL (62.4°N) and varied slowly on timescales of 10–20 min, while the higher latitude current was very variable in its intensity and location on timescales of 10 min or less. This two-component current configuration is suggestive of the "double auroral oval" described by *Elphinstone and Hearn* [1992] and *Elphinstone et al.* [1993]. Final recovery of the magnetic disturbance was in progress by ~2340 UT for the poleward current system and by ~2350 UT for the equatorward currents.

We now discuss data from the EISCAT radar system, obtained using the SP–UK–CONV experiment in which the VHF

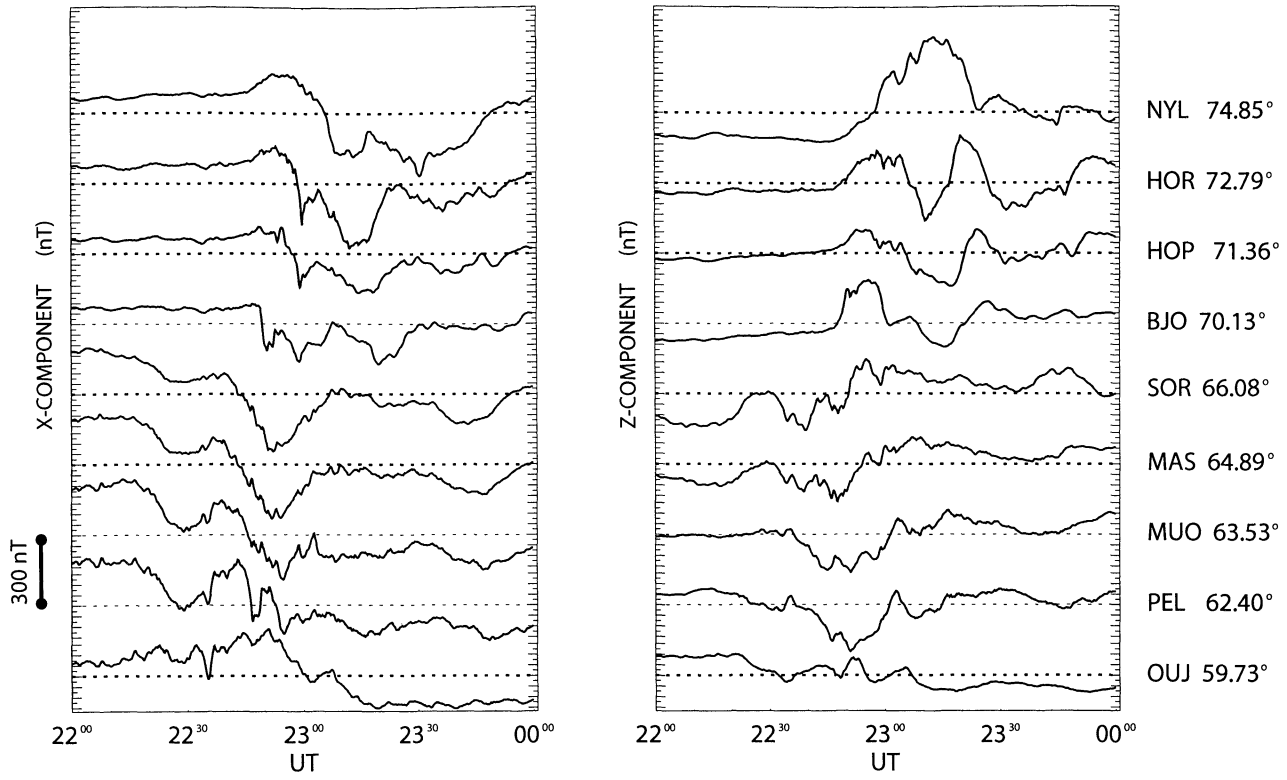

Figure 2. IMAGE magnetometer chain data for 2200–2400 UT on December 7, 1992. (left) *X* component (geographic northward) of the magnetic field and (right) *Z* component (vertically downward), from which the quiet-day means have been subtracted, indicated by the dotted zero lines. The station names and their magnetic latitudes are shown on the right of the panels.

radar was used in a split-beam mode. One pair of panels of the antenna were phased to form a beam pointed along an azimuth of 344.8° relative to geographic north (the "west" beam, beam 1), while the other pair of panels were phased to form a beam at azimuth 359.8° (the "east" beam, beam 2). The elevation angle of both beams to the local horizontal was 30°. Data were taken simultaneously at each azimuth with 10 s resolution. Echoes were received from range gates 65.3 km in length along the beams passing through the *F* region ionosphere. Useful data were acquired from the first seven gates, centered on altitudes between 283 and 509 km and covering invariant latitudes 71°–74°. The dotted lines drawn from the transmitter site at Tromsø in Figure 1 show the beam directions relative to the IMAGE magnetometer stations, while the solid portion of those lines indicate the range over which useful return signal was acquired from the *F* region ionosphere. The latter range corresponds approximately to the locations of the lower Svalbard magnetometers BJO, HOP, and HOR. We note in particular that station BJO lay directly beneath beam 2 of the radar (between the centers of gates 2 and 3).

Plates 1 and 2 illustrate the electron and ion temperature observed along each radar beam in gates 1–7 for the same interval as the IMAGE data shown in Figure 2. Plate 1a shows the *F* region electron temperature for beam 1 (344.8°). It is clear that a major change in the electron temperature propagated poleward across the radar field-of-view between 2250 and 2255 UT. The electron temperature was typically below 1400 K at all latitudes prior to the increase. After the increase, values were generally 2000–3000 K. Plate 2a shows the corresponding electron temperature for beam 2 (359.8°) from which it is evident that the enhancement occurred nearly simultaneously on both beams (though ~30 s later on beam 2 than on beam 1, as will be discussed below). As in the study by *Persson et al.* [1994a, b], we here take the electron heating of the *F* region plasma to be an indicator of soft electron precipitation and thus a proxy for auroral activity. We therefore take the electron temperature data to indicate that the poleward boundary of a substorm auroral bulge, initiated by the lower-latitude substorm intensification at ~2240 UT, propagated poleward along the radar beams between ~2250 and ~2255 UT. No simultaneous auroral data exist which address this issue directly, though an auroral image obtained by the Freja spacecraft at ~2335 UT (and shown in Figure 7 of *Fox et al.* [1999]) is consistent with this inference. At the latter time the poleward current system of the "double-oval" configuration, which was formed by the poleward expansion discussed here, appears to have been centered between NAL and HOR, at ~74°. Correspondingly, though the auroral image does not quite extend to the early morning sector occupied by IMAGE and EISCAT, it nevertheless indicates a very broad region of UV emission in the midnight sector extending from ~60° to ~73°, thus spanning essentially the same latitude range as the current system. Furthermore, as will be shown in detail below, the appearance of the electron temperature enhancement at a given latitude coincides very closely (to within a few tens of seconds) with the onset of magnetic disturbance at that latitude. We therefore believe it reasonable to infer that the poleward propagating electron temperature boundary observed in the EISCAT data is directly indicative of a similarly poleward propagating boundary of a substorm auroral bulge and electrojet current system. The

region equatorward of the boundary will hence be referred to as the "substorm-disturbed region" in the discussion below.

The ion temperature data from beam 1 shown in Plate 1b, reveals a latitudinally confined (~1°) poleward propagating ion temperature enhancement, which first appeared at the lowest latitudes at ~2248 UT. This enhancement coincided approximately with the onset of the electron temperature enhancement and the spike-like perturbation observed in the IMAGE magnetic field data (the precise relationships will be investigated in the following sections). The transient ion temperature enhancement is thus also inferred to be associated with the poleward propagating poleward boundary of the substorm-disturbed region. The data for the other beam (359.8°) in Plate 2b show the same feature (but again ~30 s later in time as will be shown below). The origins of the elevated ion temperatures will be discussed more fully in the following section, where it will be argued on theoretical grounds that the only reasonable explanation is in terms of ion-neutral frictional heating due to elevated plasma flow speeds, in line with previous studies [e.g., *St. Maurice and Hanson*, 1982; *Davies et al.*, 1997]. The EISCAT data shown in Plates 1 and 2 are thus taken to indicate that a narrow band of enhanced ion temperature is located at the poleward edge of the poleward propagating substorm-disturbed region, indicative of elevated flow speeds in this region. In the following section we undertake a more detailed study of the EISCAT data to more precisely determine the relationships between the ion and electron temperature enhancements.

3. Relationship of Ion and Electron Temperature Enhancements

In this section we focus on the temporal and spatial relationships between the ion and electron temperature enhancements observed in the EISCAT data and also make an initial examination of the line-of-sight velocity data. Complementary presentations of the temperature data are shown in Figures 3 and 4. In Figure 3 we show temperature and line-of-sight velocity data for various gates and beams versus time for the interval 2240–2300 UT. Data from gates 1, 3, and 5 are shown in Figures 3a, 3b, and 3c, respectively. The top two panels of each figure show the ion (thick line) and electron (thin line) temperatures for beam 1 (top panel) and beam 2 (middle panel). The bottom panels show line-of-sight velocity data which will be examined later in this section. Looking first at the top panels for beam 1, it can be seen that the electron temperature increased from a background level of ~1200 K to considerably higher values of ~3000 K at 2250:45 UT in gate 1, 2251:25 UT in gate 3, and 2253:35 UT in gate 5. Recalling that the centres of the gates are separated by 65.3 km in range along the beams, or ~59 km perpendicular to the local magnetic field (the angle of the radar beams is ~65° relative to the field direction), this propagation implies a poleward field-perpendicular phase speed of the boundary along the beam of ~1.4 km s^{-1}. A more precise analysis will be presented in the next section. Essentially, similar features are seen in the data

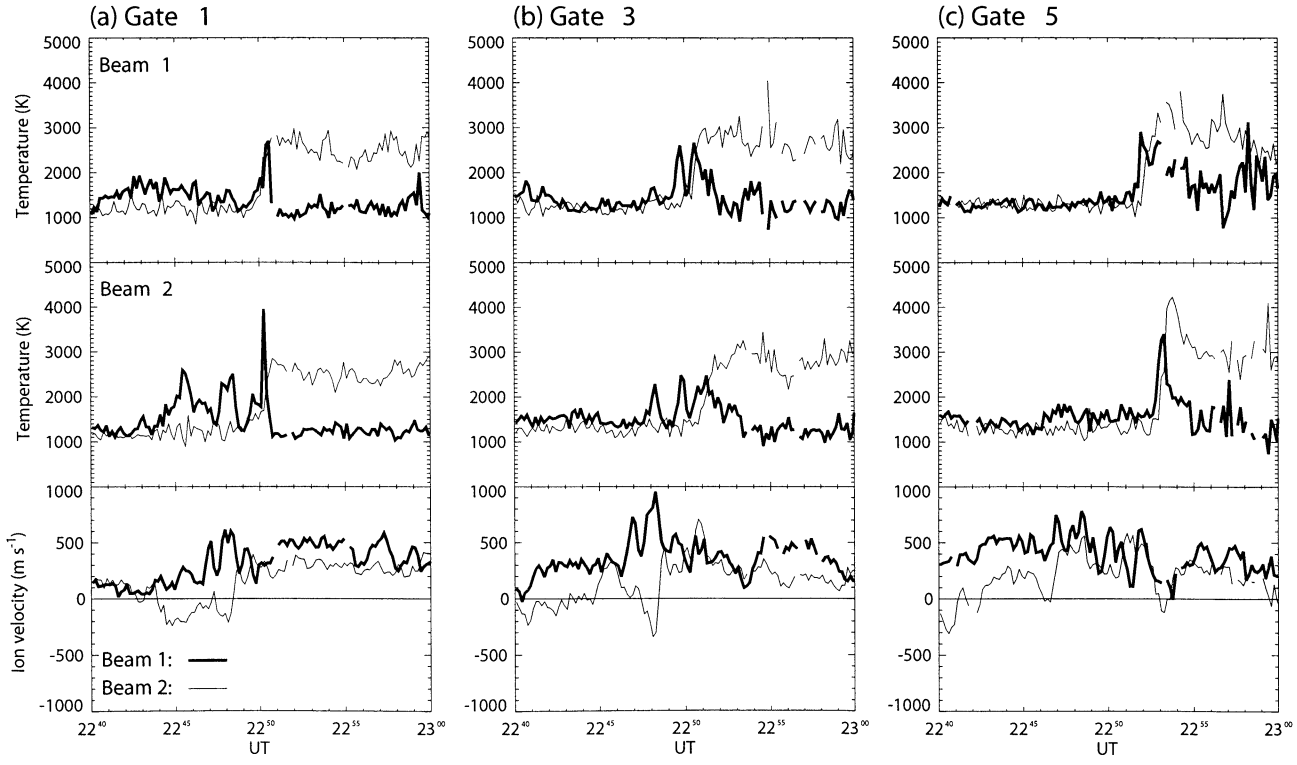

Figure 3. The electron temperature, ion temperature, and line-of-sight (LOS) velocity for both EISCAT beams for range gates (a) 1, (b) 3, and (c) 5. In each part of the figure the top and middle panels present the ion temperature (thick line) and electron temperature (thin line) for beams 1 and 2, respectively. The bottom panel presents the LOS velocity for beam 1 (thick line) and beam 2 (thin line).

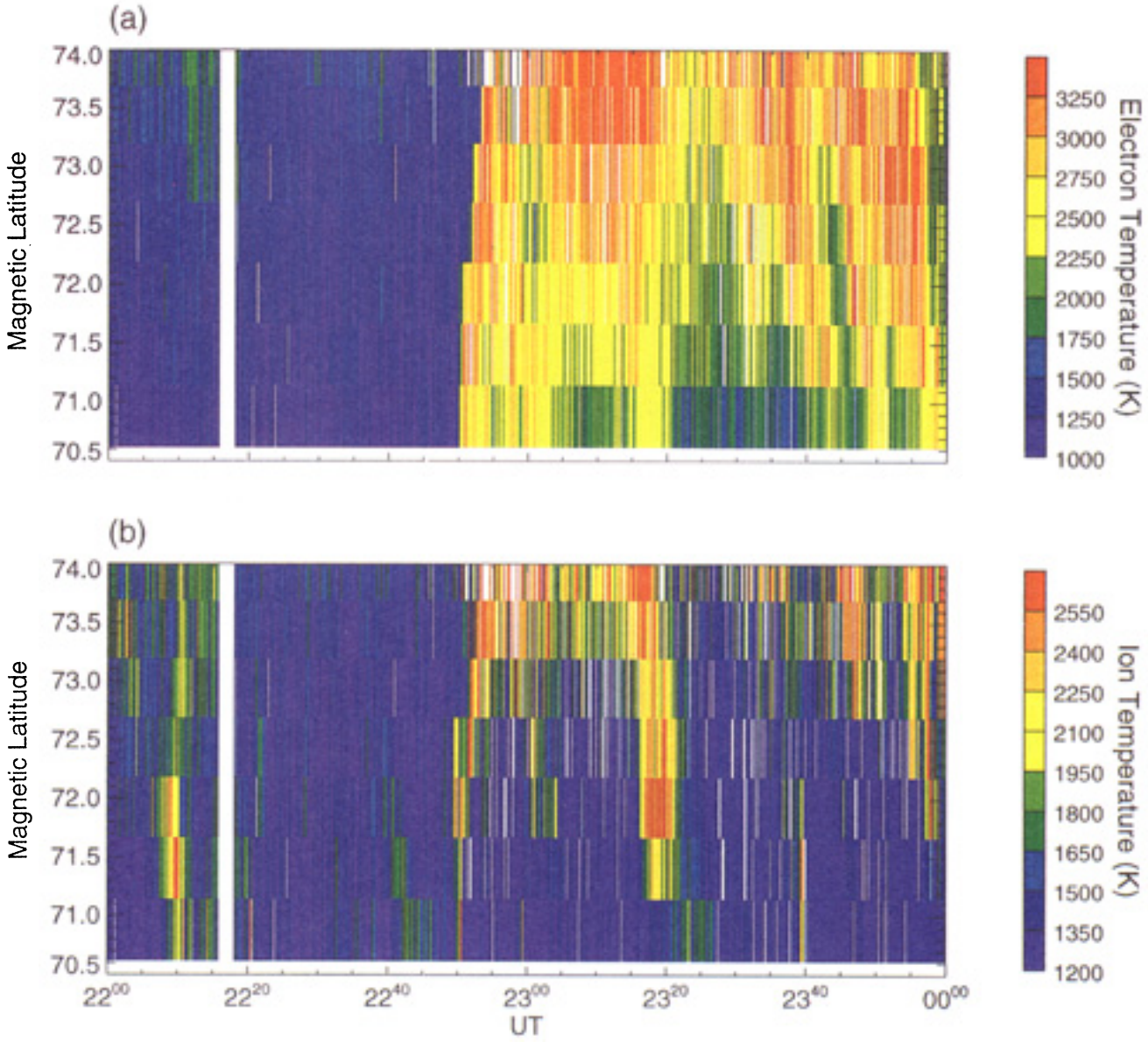

Plate 1. EISCAT VHF radar data obtained from the SP-UK-CONV experiment from 2200 to 2400 UT on December 7, 1992: (a) electron temperature data from beam 1 (344.8° geographic azimuth) and (b) ion temperature data from beam 1. The color coding represents the temperature (Kelvin) according to the scales on the right-hand side.

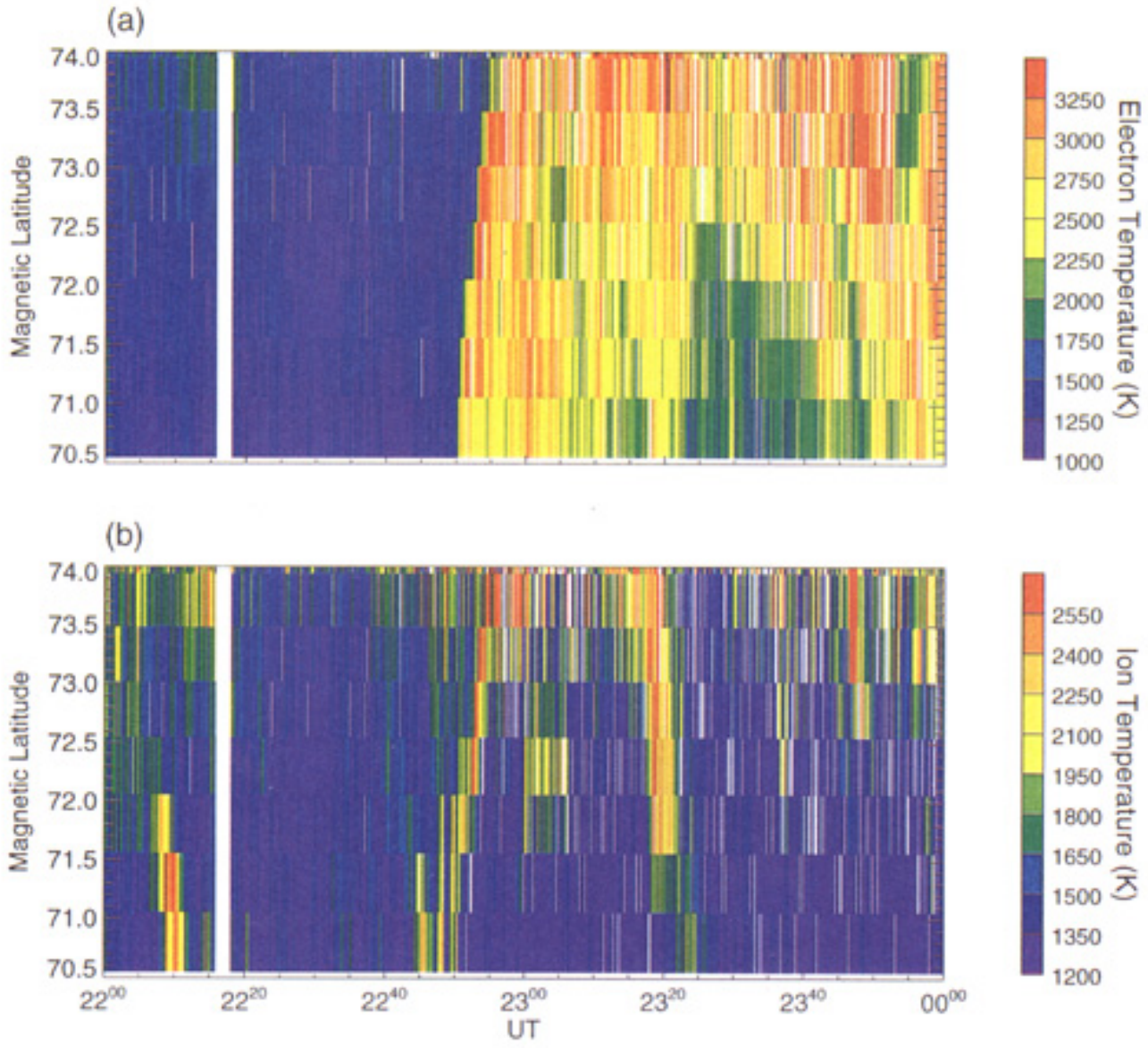

Plate 2. EISCAT (a) electron and (b) ion temperatures from beam 2 (359.8°) in the same format as Plate 1.

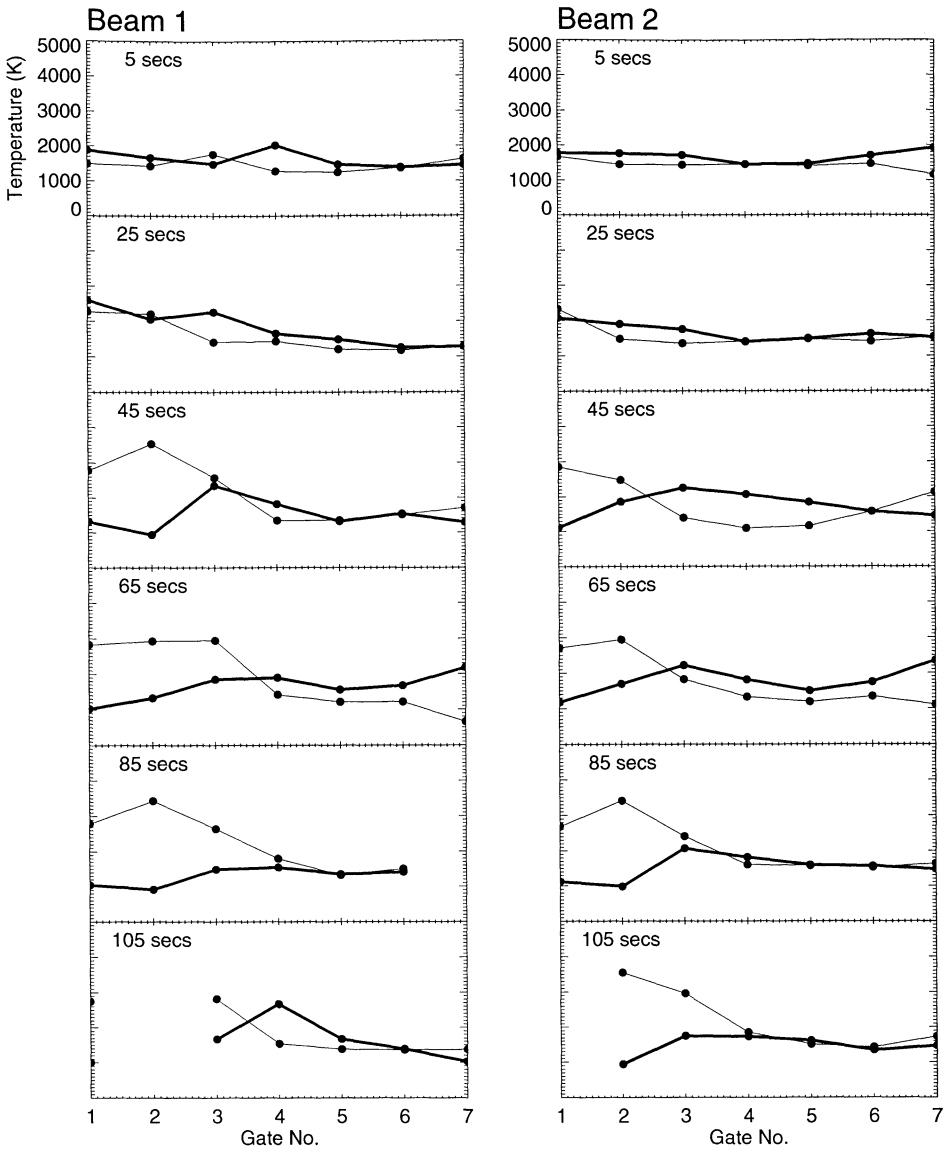

Figure 4. Plots of the ion (thick line) and electron (thin line) temperature versus range along the radar beams during the poleward passage of the electron temperature enhancement, for every other 10 s integration interval between that centered 5 s after 2250 UT (i.e., at 2250:05 UT) and 225 s after 2250 UT (i.e., at 2253:45 UT). The plots on the left-hand side are for beam 1, while those on the right are for beam 2.

from beam 2 in the middle panels, except that the increases in electron temperature occurred at slightly later times from those in beam 1. This indicates that the feature is oriented at an angle to the bisector of the two beams, with the normal tilted to the east of north (as will also be quantified later). The main change in electron temperature took place in each gate in ~50 s, which we note is essentially the timescale for a sheet boundary to propagate poleward across the ~60 km field-perpendicular width of the gate at ~1.4 km s^{-1} (~45 s). We therefore infer that the electron temperature boundary had a latitudinal thickness comparable with or less than the width of the radar range gates and hence is essentially spatially unresolved in these measurements. Following the rapid increase, the electron temperature then remained at elevated levels for the remainder of the interval shown.

The ion temperature enhancement is then seen as a ~150 s wide feature straddling the electron temperature enhancement in each gate, in which the temperature rose from ~1200 to ~2500–3000 K over an interval of ~110 s, and then fell again over ~40 s. The detailed nature of the increase varied from gate to gate. However, it began in each case before the electron temperature started to rise, typically by ~80 s, such that the ion temperature briefly exceeded the electron temperature at the start of the event in each gate. It then peaked generally near the central time of the electron temperature increase, and then fell during the subsequent interval during which the final electron temperatures were reached. Taking account of the averaging nature of the ~60 km wide radar range gates, these measurements are consistent with a layer of total width ~180 km (approximately three gates). The temperature increased over

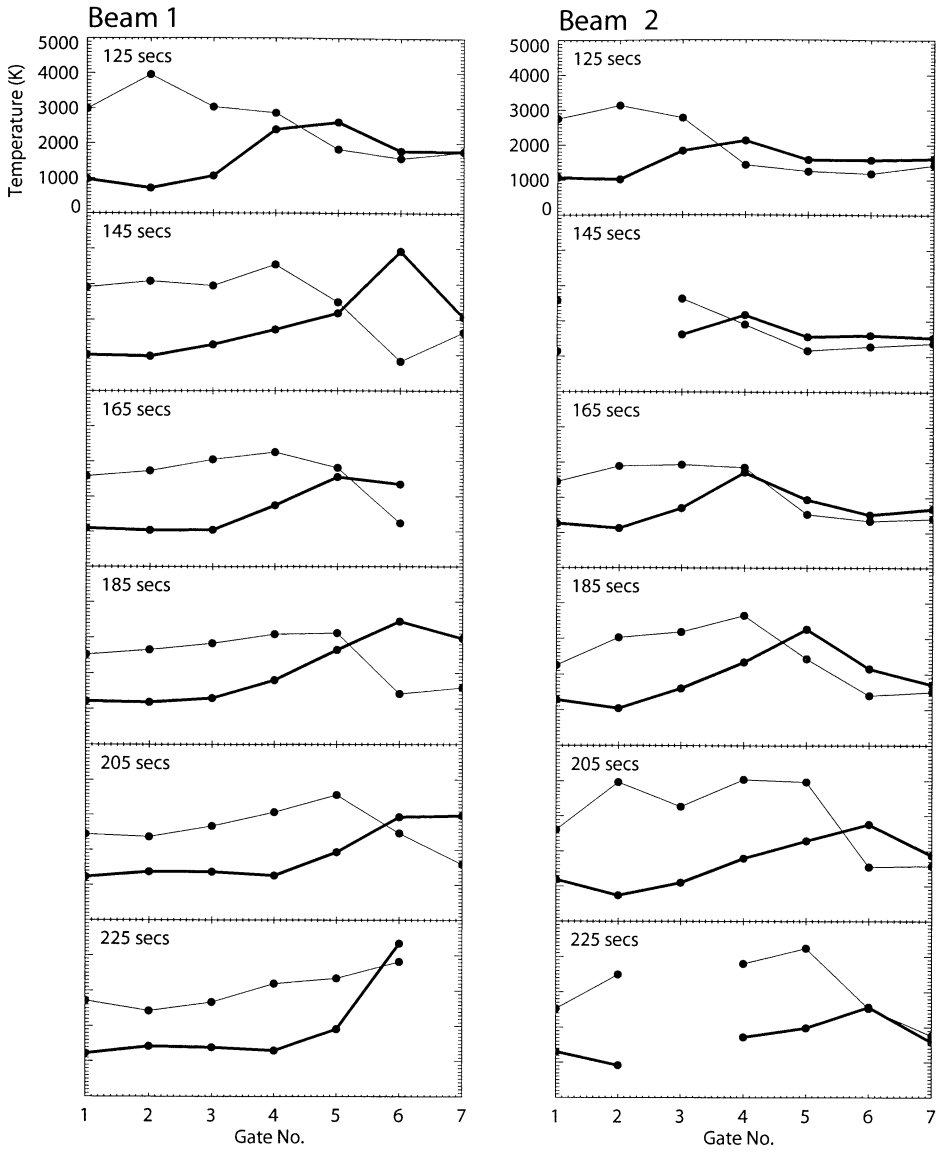

Figure 4. (continued)

~120 km (approximately two gates) poleward of the electron temperature boundary, peaked near the latter boundary, and then fell more precipitately over ~60 km (approximately one gate) in the region of high electron temperatures. The uncertainty in these estimates is plus or minus half a gate (~30 km).

Confirmation of these conclusions is shown in Figure 4 where we show the spatial structure along the radar beams for every other 10 s integration interval between that centered 5 s after 2250 UT (i.e., at 2250:05 UT) and 225 s after 2250 UT (i.e., at 2253:45 UT). The plots on the left-hand side are for beam 1 while those on the right are for beam 2. Data are shown for gates 1 to 7, where the thick line in each panel shows the ion temperature, and the thin line shows the electron temperature. If we look first at the electron temperature data it can be seen that generally only one data point lies at intermediate values across the jump in temperatures. This is consistent with our inference above that the electron temperature boundary is relatively thin, less than the ~60 km field-perpendicular width of the radar range gates. The ion temperature enhancement is then observed typically in approximately three adjacent gates (in the range 2–4), consistent with spatial scales ~180 km transverse to the field. The enhancement generally begins approximately one to two gates before the electron temperature starts to rise, peaks in the gate corresponding to the intermediate electron temperature value as it rises, and then falls more precipitately over one following gate within the region of high electron temperatures. As indicated above, while the spatial structure of the region of elevated ion temperature is thus not fully resolved in these measurements, they are consistent with a layer approximately two gates wide (~120 km) poleward of the electron temperature enhancement, and approximately one gate wide (~60 km) equatorward of it.

We now wish to discuss possible causes of the ion temperature increase from a theoretical viewpoint. The first possibility to be considered is that the data do not represent true measurements of the ion temperature but instead are produced by strong plasma velocity shears within the radar scattering volume. It has been pointed out by *Swartz et al.* [1988], for ex-

ample, that if the line-of-sight plasma velocity in the scattering volume varies by a significant fraction of the ion acoustic speed, then the typical double-humped incoherent scatter spectrum will become smeared out and flattened by the associated multiple Doppler shifts. When interpreted by the standard incoherent scatter analysis algorithms, such as we have employed here, these spectra yield ion temperatures which are far too high, and electron temperatures which are far too low, such that the derived ion temperature may then erroneously exceed the electron temperature. Brief intervals where T_i exceeds T_e have indeed been observed in the event discussed here, as pointed out above. However, there are several reasons why, in the present case, this possibility does not represent a reasonable explanation. First, the effect described by *Swartz et al.* [1988] causes both the ion temperature to be artificially enhanced, and simultaneously the electron temperature to be artificially reduced. Our data show the first of these effects, but not the second. Indeed, shortly after the ion temperature starts to rise, so does the electron temperature, such that after ~1 min in a given gate the electron temperature exceeds the ion temperature as seen in Figure 3 above. This is not the signature expected of flow shears. Second, we have examined the radar spectra corresponding to the high T_i values for any unusual features, for example, multiple peaks or asymmetries which could arise from multiple Doppler shifts caused by variations in the line-of-sight velocity within the scattering volume. Generally, the spectra are found to resemble normal symmetric double-humped incoherent scatter spectra, with superposed noise. Third, an interpretation in terms of flow shears (or time variations of the flow) requires the existence of rapid variations in the north-south (line-of-sight) flow within approximately three consecutive radar gates (but not in adjacent gates) which are comparable to the ion-acoustic speed. That is, the flow must vary by ~1–2 km s^{-1} in volumes of order a few tens of kilometers in these gates (or on timescales short compared with the 10 s integration intervals). Given the incompressible nature of ionospheric flow, the implication is that eddies must exist in a propagating layer ~180 km wide which are themselves of order or less than a few tens of kilometers in dimension, or exist for times shorter than ~10 s, and which are of amplitude ~1–2 km s^{-1}. We know of no mechanism by which such eddies could be formed, nor of any previous evidence for the existence of such short-scale, large-amplitude structures. Furthermore, if such eddies existed as a dominant but unresolved component of the plasma flow within the layer, superposed on a mean north-south flow of a few hundred m s^{-1}, we would expect to see large fluctuations in the mean line-of-sight plasma velocity within the layer, of amplitude up to ~1–2 km s^{-1}. However, the measured line-of-sight flows, such as those shown in the lower panels of Figure 3, do not show enhanced fluctuations within the high T_i layer. The flows vary at most by a few hundred m s^{-1} in this region, comparable with the fluctuations observed in the preceding interval. For all these reasons we do not believe that unresolved north-south flow shears represent a viable explanation for the high ion temperatures derived here.

We therefore proceed on the assumption that our data do indeed represent measurements of the F region ion temperature and turn to consider possible mechanisms and timescales. Following the discussion, for example, of *St. Maurice and Hanson* [1982], the ion energy equation is

$$\frac{d}{dt}\left(\frac{3}{2}p_i\right)+\frac{3}{2}p_i(\operatorname{div}\boldsymbol{V}_i)+\operatorname{div}\boldsymbol{q}_i+\mathbf{P}_i:\nabla\boldsymbol{V}_i$$
$$=\sum_n\frac{n_i m_i \nu_{in}}{m_i+m_n}\left[3k(T_n-T_i)\psi_{in}+m_n(\boldsymbol{V}_i-\boldsymbol{V}_n)^2\phi_{in}\right] \quad (1)$$
$$+n_i\nu_{ie}\left[3k(T_e-T_i)+m_e(\boldsymbol{V}_i-\boldsymbol{V}_e)^2\right],$$

where from left to right the terms on the left-hand side of the equation are the convective time derivative of the internal heat energy of ion species i with pressure p_i (assumed isotropic for purposes of initial discussion), the mechanical energy term associated with compressions and expansions of the gas (velocity $\boldsymbol{V}_i$), the heat conduction term (heat flux $\boldsymbol{q}_i$), and the viscous term (ion pressure tensor $\mathbf{P}_i$). The terms on the right describe the heat exchange between the ions (mass m_i, temperature T_i) and the neutrals (mass m_n, temperature T_n), the frictional heating due to the relative motion between ions and neutrals (velocity $\boldsymbol{V}_n$), the heat exchange between the ions and electrons (mass m_e, temperature T_e), and the frictional heating due to the relative motion between ions and electrons (velocity $\boldsymbol{V}_e$). The quantities ν_{in} and ν_{ie} are the ion-neutral and ion-electron collision frequencies, respectively, k is Boltzmann's constant, and the functions ψ_{in} and ϕ_{in} which describe the velocity dependence of the collision cross sections are to a good approximation equal to 1. At altitudes of interest (~280–470 km for gates 1–6), the ion-neutral collision time ν_{in}^{-1} is typically a few seconds, lying between ~1 s and the lower altitudes, and ~10 s at the higher altitudes, while the ion-electron collision times ν_{ie}^{-1} are considerably longer, ~300 s for atomic oxygen ions in the F region [see, e.g., *Kelley*, 1989, section 2.2].

Now for reasons previously discussed, for example, by *St. Maurice and Hanson* [1982], (1) may be considerably simplified in the F region. Specifically, with regard to the various terms from left to right in (1), (1) the mechanical term can be neglected due to the strong magnetic field which renders the gas essentially incompressible, (2) the heat conduction term acts only to modestly spread the heat energy away from a heated volume and is not generally a significant effect, (3) the viscous heating term is also small unless there are substantial shears in flow over spatial scales of a few kilometers, considered unlikely for reasons indicated above, (4) the Mass Spectrometer Incoherent Scatter neutral atmosphere model indicates that only one ion and neutral species needs to be considered at altitudes of interest (i.e., atomic oxygen), unless the flow speeds become large, (5) the heat exchange term between ions and electrons is generally negligibly small due to the small value of ν_{ie} (compared with ν_{in}), and (6) the field-perpendicular ion and electron velocities are essentially equal (and we assume no large relative drifts along the field). Assuming also for simplicity that during rapid heating the density stays approximately constant, we then have the approximation

$$\frac{dT_i}{dt}\approx\nu_{in}\left[(T_n+T_i)+\frac{m_n}{3k}(\boldsymbol{V}_i-\boldsymbol{V}_n)^2\right]. \quad (2)$$

Assuming that the neutrals represent a heat sink whose temperature will not be significantly affected, (2) can be rearranged to give

$$\frac{d(T_i-T_n)}{dt}+\nu_{in}(T_i+T_n)\approx\frac{m_n\nu_{in}}{3k}(\boldsymbol{V}_i-\boldsymbol{V}_n)^2, \quad (3)$$

with the solution

$$T_i-T_n\approx\int_{-\infty}^{t}dt'e^{-\nu_{in}(t-t')}\left[\frac{m_n\nu_{in}}{3k}(\boldsymbol{V}_i-\boldsymbol{V}_n)^2\right]. \quad (4)$$

The elevation of the ion temperature above the neutral temperature is therefore given by a convolution between an exponential function, with a time constant ν_{in}^{-1}, and the heating term associated with ion-neutral frictional heating. It can therefore be seen that if the latter term varies slowly on timescales of order ν_{in}^{-1}, that is, on timescales longer than a few seconds, then it can be taken to be constant over the interval that the exponential function has appreciable values. Integration then yields the quasi-steady approximation

$$T_i - T_n \approx \left(\frac{m_n}{3k}\right)(\boldsymbol{V}_i - \boldsymbol{V}_n)^2 , \tag{5}$$

which is just the simplified form of (1) with all the terms on the left-hand side set equal to zero. Alternatively, if the ion-neutral frictional heating term changes sharply, then the ion temperature changes exponentially to the value given by (5) on the timescale ν_{in}^{-1}, that is, in a few seconds.

Now in the present case the boundary of the substorm-disturbed region propagated poleward at ~1.4 km s^{-1}, while, as will be shown below, the plasma in the Earth's rest frame flowed equatorward at a few hundred m s^{-1}. Consequently, in the rest frame of the boundary, the plasma flowed from the poleward to the equatorward sides of the boundary at a relative speed of somewhat less than ~2 km s^{-1}. Given the ~200 km spatial extent of the layer of elevated ion temperatures, the time taken to flow through the structure was therefore ~100 s. This value is between 1 and 2 orders of magnitude longer than the exponential timescales for ion heating and cooling in the F region ionosphere. Consequently, we may expect the steady state formula given by (5) to be a good approximation.

The above discussion indicates that the only reasonable explanation of the layer of high ion temperature is that there must have existed a layer of high ion velocity in the vicinity of the boundary which elevated the ion temperature through ion-neutral frictional heating, essentially in situ. However, in applying (5) to the data, some complicating factors need to be borne in mind. The first is that the energy input to the ions in this case is predominantly into the field-perpendicular velocity components, so that at high relative drifts the ion distribution function becomes anisotropic, with different temperatures parallel and perpendicular to the field ($T_{i\parallel}$ and $T_{i\perp}$, respectively). The ion temperature in (5) is then the average, "three-dimensional" temperature given by $T_i = (T_{i\parallel} + 2T_{i\perp})/3$, while the temperature observed by the radar along the line of sight is the "one-dimensional" temperature given by $T_{i\,los} = T_{i\parallel}\cos^2\Phi + T_{i\perp}\sin^2\Phi$, where Φ is the angle of the radar beam to the field direction, equal to ~65° in the present case [e.g., *Lockwood et al.*, 1988, 1993]. In terms of the field parallel and perpendicular energy partition coefficients $\beta_\parallel$ and $\beta_\perp$, the parallel and perpendicular temperatures are given by

$$\begin{aligned} T_{i\parallel} - T_n &= \beta_\parallel \left(\frac{m_n}{2k}\right)(\boldsymbol{V}_i - \boldsymbol{V}_n)^2 \\ T_{i\perp} - T_n &= \beta_\perp \left(\frac{m_n}{2k}\right)(\boldsymbol{V}_i - \boldsymbol{V}_n)^2 , \end{aligned} \tag{6}$$

where $\beta_\perp = 1 - \beta_\parallel/2$. The relationship between the ion temperature along the line of sight and the ion velocity is then

$$T_{i\,los} - T_n = \left[\sin^2\Phi - \beta_\parallel\left(\frac{3}{2}\sin^2\Phi - 1\right)\right]\left(\frac{m_n}{2k}\right)(\boldsymbol{V}_i - \boldsymbol{V}_n)^2 . \tag{7}$$

The results shown in Figure 3 indicate that the ion temperatures within the boundary region peak at values typically ~1500 K above those measured before and after. Assuming an atomic oxygen atmosphere and ionosphere, $\beta_\parallel \approx 0.25$, and $\Phi \approx 65°$, then yields $|\boldsymbol{V}_i - \boldsymbol{V}_n| \approx 1.5$ km s^{-1}, which seems an entirely plausible value. However, at such relative velocities two additional effects need to be considered. The first is that the proportion of molecular ions (principally NO^+) in the F region may increase significantly [e.g., *Schunk et al.*, 1975]. Since the EISCAT analysis algorithm assumes solely atomic oxygen ions at these heights, the derived temperatures will then be incorrect, and given approximately by

$$T'_{i\,los} \sim \left(\frac{m_{O^+}}{\langle m_i \rangle}\right) T_{i\,los} ,$$

where m_{O^+} is the mass of an oxygen ion, and $\langle m_i \rangle$ is the mean ion mass. For an ionosphere with a significant fraction of nitric oxide ions therefore the derived ion temperature will be less than the true value by factors of up to ~1.9, this value assuming a totally molecular ion composition. The ion speeds derived directly from (7) will then be less than the true values. For example, if we take a change of ion temperature of ~3000 K as more representative, and $\beta_\parallel \approx 0.5$ for nitric oxide, then (7) gives $|\boldsymbol{V}_i - \boldsymbol{V}_n| \approx 2$ km s^{-1}. However, for the peak flow speeds appropriate here (~1–2 km s^{-1}), molecular ions are likely to make a significant contribution only in the lowest two range gates, below ~350 km, and since the effect on the estimated relative flow speeds is not large, we will not consider this effect further. Finally, the ion flow speeds we have just estimated are comparable with the inferred neutral oxygen thermal speed, ~1 km s^{-1}. Under these conditions the ion distribution may not only become anisotropic but may also develop non-Maxwellian (toroidal) features about the field direction. If the incoherent backscatter spectra are then interpreted in terms of Maxwellian distributions, as in the conventional analysis employed here, the inferred ion temperatures will be larger than the true values (the effect thus having the opposite sense to the composition effect just discussed), while the electron temperatures will be smaller. This effect has been modeled, for example, by *Raman et al.* [1981], with results which indicate only modest temperature inaccuracies (around a few 100 K) for the conditions prevailing during this study. Again therefore this effect will not be considered further, and for the purpose of approximate estimation of flow speeds from observed temperature data, (7) will thus be used directly.

Given the above conclusions it thus becomes of interest to examine the velocity data during the interval that the boundary propagated along the radar beam. However, we should point out immediately that the geometry of the radar experiment is not ideal to examine these flows. If the boundary is an approximately planar structure on scales of several 100 km, directed principally east-west, then the incompressibility of the ionospheric flow guarantees that any enhanced flow near the boundary must be directed along it, approximately east-west, while the flow across the boundary, approximately north-south, must be continuous. However, in the SP-UK-CONV experiment employed here the two radar beams point approximately northward and are only separated in angle by ~13° in the beam plane, as shown in Figure 1. Consequently, the line-of-sight velocities observed along these beams will both be sensitive to the north-south flow approximately transverse to the boundary,

while being relatively insensitive to the east-west flow approximately along the boundary. Indeed, an east-west flow enhancement of ~1.5 km s^{-1} as anticipated above will produce a flow of less than ±200 m s^{-1} along the line of sight of the two beams. It is nevertheless important to carefully examine these data to see what information can be retrieved.

Line-of-sight velocity data are thus shown in the bottom panels of Figure 3 for gates 1, 3 and 5, where positive velocities are directed toward the radar. Data for beam 1 are shown by the thick line, while those for beam 2 are shown by the thin line. In the simplest interpretation of this data it is assumed that the flow velocity vector in the ionosphere has the same magnetic north-south and east-west components at a given magnetic latitude, independent of longitude. In terms of the geometry of this experiment, this means that the flow components are assumed to be essentially identical in the ionosphere in equivalent gates on the two beams, which are very nearly at the same magnetic latitudes. With this assumption the mean value of the two line-of-sight velocities shown in the bottom panels of Figure 3 indicates the flow along the beam bisector, while the difference indicates the flow transverse to the bisector. Thus, for example, a mean speed which is positive indicates equatorward flow along the bisector, while if the line-of-sight velocity is larger on beam 1 than on beam 2, it also has an eastward component. More precisely, the flow along the bisector in the beam plane is v_b (positive equatorward), and the flow transverse to the bisector is v_t (positive eastward) where

$$v_b = \frac{(v_1 + v_2)}{2\cos(\varphi/2)} \quad v_t = \frac{(v_1 + v_2)}{2\sin(\varphi/2)}, \tag{8}$$

where v_1, v_2 are the velocities along beams 1 and 2, respectively, and φ is the angle between the beams in the beam plane, equal to 12.99°.

Examining the velocity data in Figure 3 with this in mind, it can be seen that v_1 (thick line) is almost exclusively positive during the interval, while v_2 is usually smaller (except for brief intervals near the boundary crossing itself), and occasionally negative. This implies that during the interval shown the flow is generally directed eastward and equatorward. We note in particular that the mean velocity generally increased during the early part of the interval, prior to the arrival of the boundary, implying that the equatorward flow was enhanced in the interval following the substorm intensification onset at 2240 UT. Temporal surges of eastward flow, with coincident enhancements in the ion temperature, also occur in this interval, such as that peaking at 2248 UT in gates 1 and 3, just before the arrival of the boundary in these lower gates. Indeed, the flow is very variable in all gates and on both beams following ~2245 UT and prior to the arrival of the boundary and appears to have a quasi-oscillatory behavior, with evidence of westward flows, for example, at ~2251 UT. After the boundary has passed over a particular gate, however, the flows become noticeably steadier, and directed eastward and equatorward, consistent with a westward directed Hall electrojet within the substorm-disturbed region.

Now although such an interpretation of the velocity data may be sufficient to draw overall conclusions about the flow, such as those outlined above, it is clearly insufficient to examine the details of the flow within the propagating boundary region itself, as required to investigate the origins of the ion temperature enhancements. The principal difficulty is that because the boundary is tilted relative to the bisector of the radar beams, the layer of heated ions and inferred elevated flow speeds passes through a given gate on the two beams at different times, as is clearly seen in Figure 3. This fact therefore immediately invalidates the assumption, at least in the boundary region, of corresponding flows in equivalent gates of the two beams. In this case a more sophisticated analysis of the velocity data is required, in which the line-of-sight velocities are combined in a boundary-aligned coordinate system, assuming that the flow varies principally in the direction orthogonal to the boundary. Such an analysis is presented in the next section.

4. Analysis of Line-of-Sight Velocity Data

In the previous section we inferred from an examination of ion and electron temperature data that a region of high-speed flow, ~1–2 km s^{-1}, existed in a layer ~180 km (approximately three radar gates) wide at the poleward boundary of a poleward expanding substorm-disturbed region. In this section we analyze the EISCAT velocity data for direct evidence of these flows. To do this we need to combine the line-of-sight velocities along each radar beam to determine the north-south and east-west components of the flow from the sums and differences of the line-of-sight (LOS) values, as indicated above, but employing a boundary-aligned coordinate system on the assumption of a flow organized relative to a quasiplanar boundary. An analysis of this nature is now presented. However, we note that this is not a guaranteed procedure. Because the two beams of the radar experiment are pointed principally northward and separated in angle by only ~13° in the beam plane, the data are relatively insensitive to the flow along the boundary, with expected effects in the line-of-sight velocity of only a few hundred meters per second, as pointed out above. Significant variations from planar conditions along the boundary on spatial scales of ~100–200 km (the east-west separation of the beams in the relevant radar gates), will then invalidate the analysis. Nevertheless, the method seems worthy of exploration and is shown to produce plausible results provided that the data are screened to ensure similar conditions on the two beams of the radar, as will be described further below.

The first step in the analysis is to determine the location of the boundary as a function of time as it propagated along the radar beams. It can be seen from Figure 3 that the electron temperature time series provides a clear and consistent determination of the time that the precipitation boundary passed through a given radar range gate, with the time at which a value of 2000 K was recorded being a good central time of the change in each gate. For definiteness we therefore take the time at which the measured electron temperature passed through 2000 K to be the time at which the boundary was located centrally within a given radar range gate. Figure 5 shows the propagation of the boundary defined by this measured electron temperature along each beam, where the solid line corresponds to beam 1 and the dashed line corresponds to beam 2. We have plotted the time (on the horizontal axis) at which 2000 K was measured in each gate versus the range along the beam of that gate (on the vertical axis), for the first six gates along each beam, as numbered. It can be seen that this temperature was observed in a given gate of beam 1 some 20–50 s before it was observed in the equivalent gate of beam 2, implying that the boundary normal was inclined east of north away from the bisector of the radar beams, as indicated above. By linearly interpolating between each data point along a given

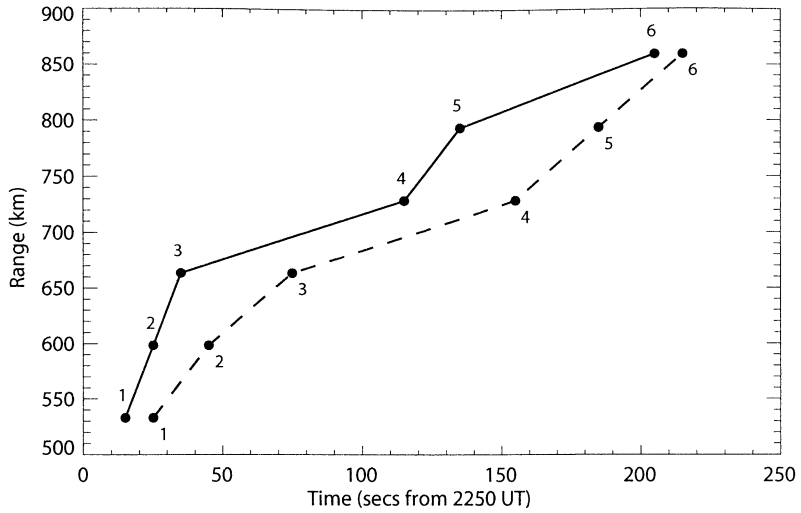

Figure 5. Range of the 2000 K T_e measurement along each radar beam as a function of time, determined from the time series for each radar gate, as numbered. The solid line is for beam 1 (geographic azimuth 344.8°), while the dashed line is for beam 2 (geographic azimuth 359.8°).

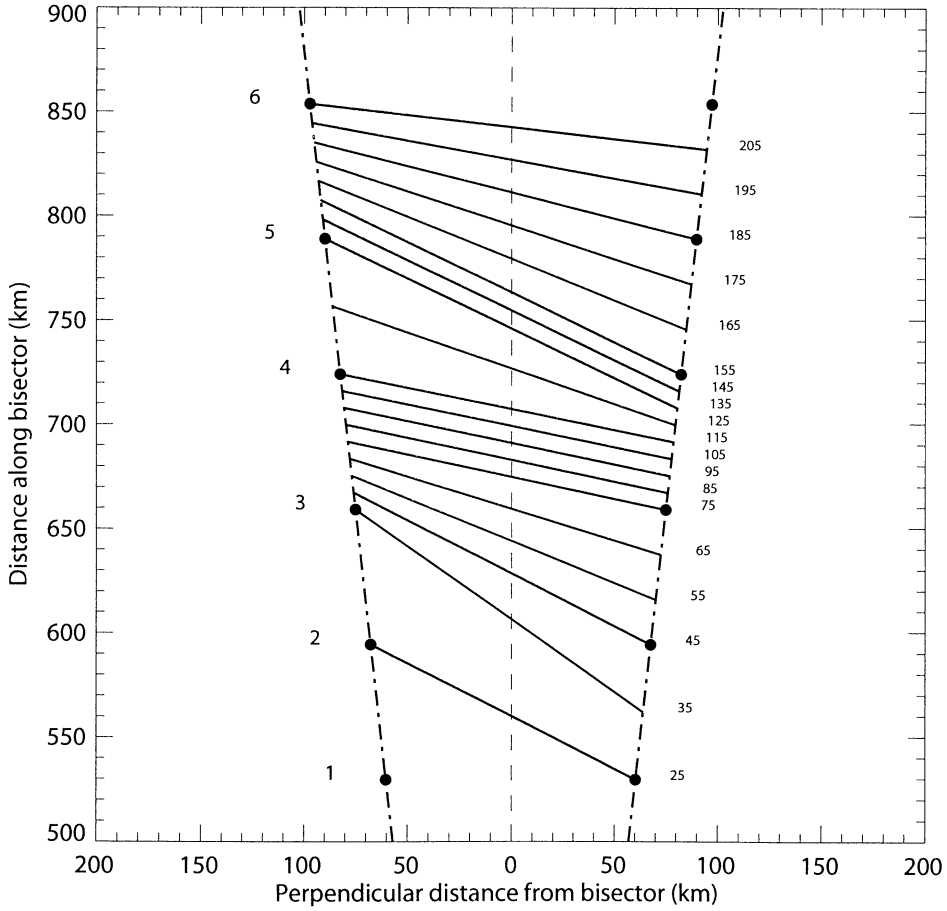

Figure 6. Location of the 2000 K T_e boundary in the radar beam plane at 10 s intervals from 25 s after 2250 UT to 205 s. The position along each beam at each time is obtained from Figure 5, and a linear variation is assumed between them. The dashed lines indicate the radar beams, and the numbered dots are the centers of each gate from 1 to 6.

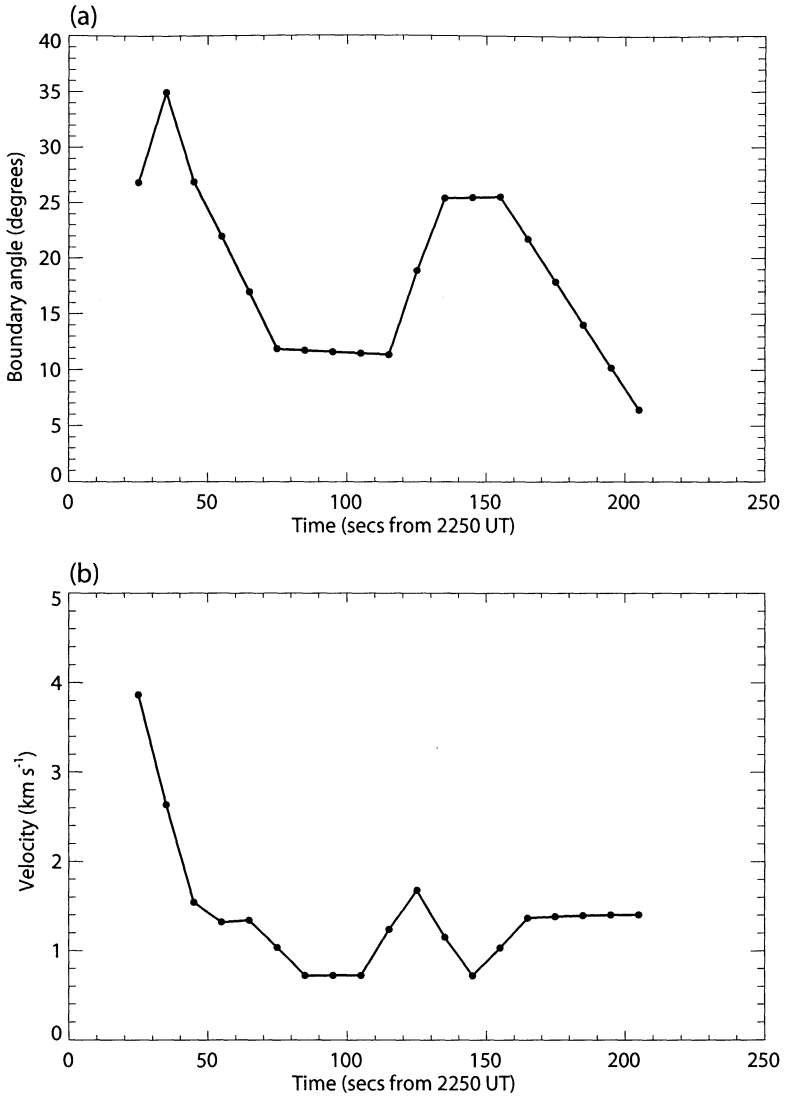

Figure 7. (a) Angle of the normal of the 2000 K T_e boundary to the bisector of the radar beams in the beam plane obtained from the results shown in Figure 6. Positive values indicate that the normal is rotated east of the bisector as seen in the latter figure. (b) Propagation speed of the boundary along its three-dimensional normal at the radar beam bisector location. The three-dimensional orientation of the boundary has been determined from its cut through the beam plane shown in Figure 6 assuming that it is also aligned with the local magnetic field. The values are reduced only by a small factor (less than 10%) from the direct one-dimensional speed along the bisector in the beam plane.

beam, we can then estimate the boundary position as a function of time along the beam. We then combine the data from the two beams to determine the boundary orientation as a function of time, assuming that the boundary was planar within the EISCAT field of view. Figure 6 thus shows the boundary position in the beam plane at 10 s resolution over the interval during which the 2000 K T_e value was observed on each beam. This interval was from 2250:25 to 2253:25 UT (i.e., from 25 to 205 s after 2250 UT as marked in the figure), an interval of 3 min (the central times of each 10 s integration interval are quoted here). It is only during this interval that the plasma velocity in the vicinity of the boundary can be investigated. From these results both the orientation and the velocity of the boundary may be determined, as shown in Figure 7. Figure 7a shows the angle of the normal to the boundary in the beam plane relative to the beam bisector, directed positive eastwards. This varied between ~10° and ~35° over the interval shown, with a typical value of ~20°. Figure 7b shows the propagation speed of the boundary along the boundary normal at the beam bisector position. The three-dimensional boundary normal vector has been obtained by projecting the cut in the beam plane at any time, as shown in Figure 6, along the local magnetic field direction. The normal velocity so determined averaged ~1.5 km s^{-1}, compatible with the value estimated more simply above. Its value is generally only a modest factor (less than ~10%) smaller than the one-dimensional speed of the boundary along the bisector in the beam plane that would be determined directly from the propagation that is evident in Figure 6.

Using the boundary position for each 10 s data interval, we have then used (8) to combine interpolated line-of-sight veloci-

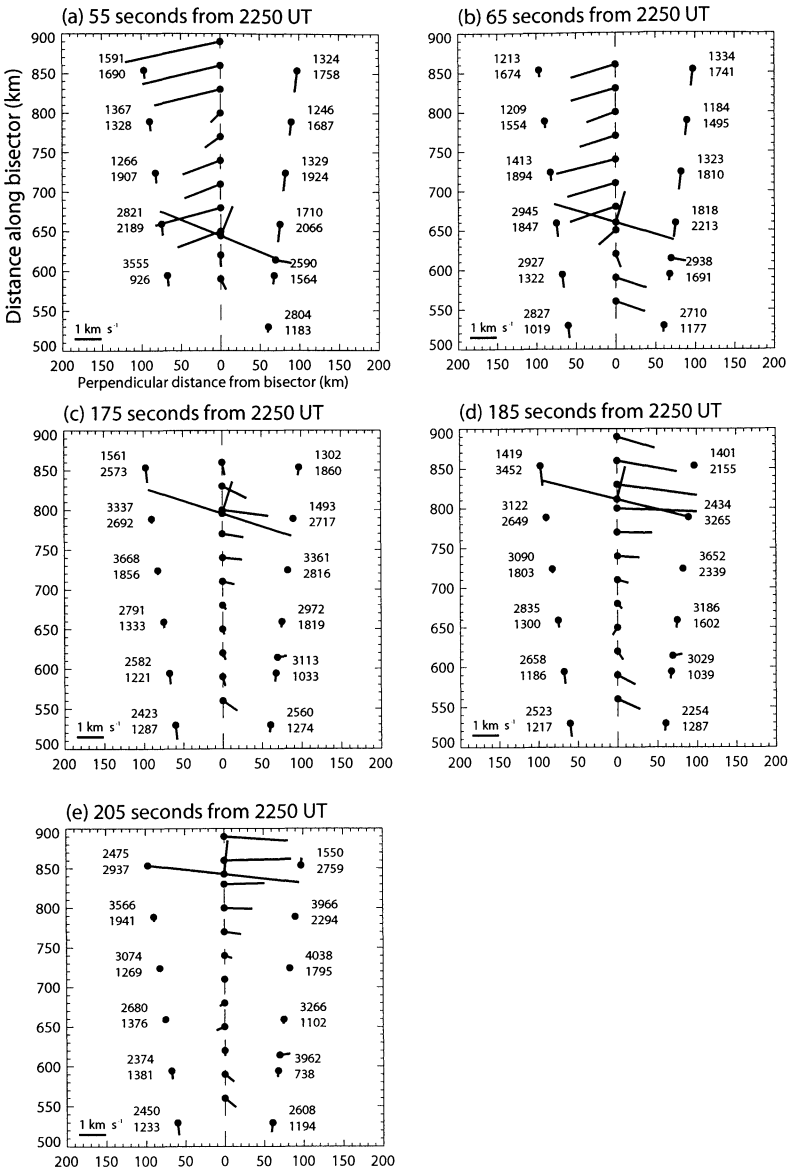

Figure 8. Plasma flow vectors in the beam plane determined by combining line-of-sight velocities at points on the two beams which are equidistant from the instantaneous electron temperature boundary. Specifically, vectors have been derived at spatial points separated by 30 km along the bisector, using line-of-sight velocities suitably interpolated between range gates on the two beams according to the instantaneous orientation of the boundary during the 10 s measurement interval, as in Figure 6. The vectors are plotted on the bisector of the radar beams. The actual line-of-sight velocities measured are also plotted, using the same scale, at the centers of the range gates along the two beams, indicated by dots. The numbers associated with each gate give the electron temperature (top) and ion temperature (bottom), in Kelvin. The instantaneous orientation of the 2000 K T_e boundary is also shown, drawn as a straight line between the radar beams as in Figure 6, together with its velocity at the bisector. The velocity shown is the three-dimensional velocity along the normal, projected onto the beam plane. The vector shown between gates 2 and 3 of beam 2 is a pseudoflow vector determined from the horizontal magnetic perturbation at BJO, assuming that the ground magnetic disturbance is wholly due to Hall currents in an ionosphere with a nominal conductivity of 10 mho. The vector has again been projected onto the beam plane and has been drawn at a point which is connected along the local magnetic field with the point 110 km vertically above BJO. Five panels of results are shown, corresponding to the 10 s measurement intervals centered 55, 65, 175, 185, and 205 s after 2250 UT. It was only for these intervals that the results were not compromised either by clear evidence of dissimilar flows on the two beams (as indicated by the ion temperature data) or by data gaps.

ties at points along the two beams which were parallel to the instantaneous boundary. These points are taken to be equivalent points at which the flow vectors were identical. The beam plane flow vectors so determined are presented as vectors located at the beam bisector and have been derived with a spatial resolution of 30 km along the bisector in order to aid the eye in following the latitudinal variations. We found that although a significant number of cases showed the anticipated flow enhancement at the boundary, this feature did not consistently emerge from the analysis. However, bearing in mind the above discussion, we then screened the results to eliminate those integration intervals in which there was direct evidence of significant differences in the total plasma velocity vector in the two radar beams. To do this we compared the ion temperature data on the two beams. As indicated above, the ion temperature is an indicator of the magnitude of the total plasma velocity vector in the frame of the neutral wind through (5) and (7), and the neutral wind is itself expected to be relatively unvarying on the space scale and timescale considered here. We thus eliminated those intervals in which there were consistent and substantial differences (by several hundred Kelvin) between the ion temperatures on the two beams in the boundary coordinate system, particularly in the vicinity of the boundary itself. When intervals compromised by data gaps are also eliminated, five integration intervals remain, two from adjacent intervals when the boundary was located in the equatorward half of the field-of-view of the radar, and three from near-adjacent intervals (separated by an interval compromised by a data gap) when it was nearing the poleward limit of data. These results are shown in Figure 8. Here we show not only the derived flow vectors in the beam plane, as just described, but also the position of the 2000 K T_e boundary and its normal velocity projected onto the beam plane (using the same velocity scale as the flow vectors). We also show the position of the center of each radar gate along the two beams (for gates 1 to 6), and the LOS velocities from which the flow vectors were derived. The two numbers associated with each gate also give the electron (top) and ion (bottom) temperatures, respectively. The vector lying between gates 2 and 3 of beam 2 shows a pseudoflow vector projected into the beam plane derived from the BJO magnetometer data, assuming that the magnetic effect is due to a uniform overhead Hall current sheet with a nominal height-integrated conductivity of 10 mho. To obtain a more appropriate magnetic baseline than was shown in Figure 2 (the daily mean), we averaged the magnetometer data over the prior quiet interval between 2200 and 2230 UT.

Figures 8a and 8b show results for the 10 s intervals centered on 55 and 65 s after 2250 UT (i.e., at 2250:55 and 2251:05 UT), when the 2000 K T_e boundary was located in the equatorward part of the radar field of view. During this interval the flow poleward of the boundary had temporarily reversed to westward and equatorward from prior eastward and equatorward flows. It can be seen that the derived westward and equatorward flows increase to a value of ~2 km s^{-1} in a layer which is ~100 km (approximately two gates) wide just poleward of the electron temperature boundary, in approximate agreement with the ion temperature data. Across the boundary the velocity vectors fall in magnitude in concert with the fall in ion temperature and rotate through equatorward toward eastward to become approximately parallel to the boundary. The eastward flows and implied westward Hall currents in the latter region are, of course, compatible with the negative X component magnetic perturbations observed by the ground magnetometers once the boundary had passed over (as will be discussed in more detail below). Here we note that the pseudoflow vector derived from BJO magnetic data was directed essentially along the boundary at this time, as expected. However, examination of the data shows that it had done so continuously for the previous ~100 s, well before the boundary itself reached BJO (at ~2250:55 UT in Figure 8a), despite the variable nature of the overhead preboundary flow. This we take to be due to the fact that the magnetometer integrates the overhead current over areas with radial dimensions of ~150 km and that it responded primarily to the currents within the high-conductivity region equatorward of the boundary, starting about 100 s before the boundary (traveling at ~1.5 km s^{-1}) appeared overhead. The currents poleward of the boundary were evidently negligible by comparison despite the relatively large flows present, thus implying very low preboundary ionospheric conductivity.

Figures 8c–8e show results for intervals when the boundary was in the poleward part of the field of view. In the first of these, centered on 175 s after 2250 UT (i.e., 2252:25 UT), the derived flow is directed equatorward in the region poleward of the boundary, and then rotates over approximately one gate to a strong eastward flow peaking at ~2 km s^{-1} in the vicinity of the boundary, in accordance with the rise in ion temperature. The flow speed then declines over approximately one gate inside the boundary in accordance with the decline in ion temperature. The results derived for the intervals centered on 185 and 205 s after 2250 UT (i.e., at 2253:05 and 2253:25 UT), shown in Figures 8d and 8e, are basically similar, but the layer of elevated eastward flow appears to be a little wider and faster, concomitant with the ion temperature data. In Figure 8c, for example, the peak elevation in ion temperature observed near the boundary was ~1600 K. Using (7) (and neglecting the neutral wind velocity), we then anticipate $V_i \approx 1.5$ km s^{-1}, which is very comparable to the elevated speeds derived in the boundary region. In Figure 8d, the peak ion temperature elevation was ~2300 K, such that $V_i \approx 1.8$ km s^{-1} is expected theoretically. This is again not dissimilar from the overall values derived in the boundary region, though the values derived at the boundary itself peak at ~3 km s^{-1}. Given the factors involved in the calculation, discussed in the previous section, this difference is probably not significant.

In summary, therefore, when our results are screened to exclude clear cases in which the ion temperatures, and by inference the plasma flows, differ significantly on the two radar beams, our algorithm retrieves the anticipated presence of enhanced flows in the vicinity of the boundary. Peak flow speeds derived are ~1.5–3 km s^{-1}, which are reasonably compatible with those expected from the observed ion temperature enhancements of ~1500–2500 K. In two cases the enhanced flow was directed westward, during an interval in which the flow poleward of the boundary of the substorm-disturbed region was also inferred, briefly, to be westward. In other cases the flow was directed eastward. In all cases the layer of highest flows was ~100–150 km (approximately two gates) wide, though the overall layer of elevated temperatures is a little wider, as previously indicated.

5. Relationship to Ground Magnetic Disturbance

In Figure 9 we finally establish more precisely the relationship between features observed in the radar data and the ground magnetic disturbance. The top panel shows the three components of the magnetic perturbation vector observed at

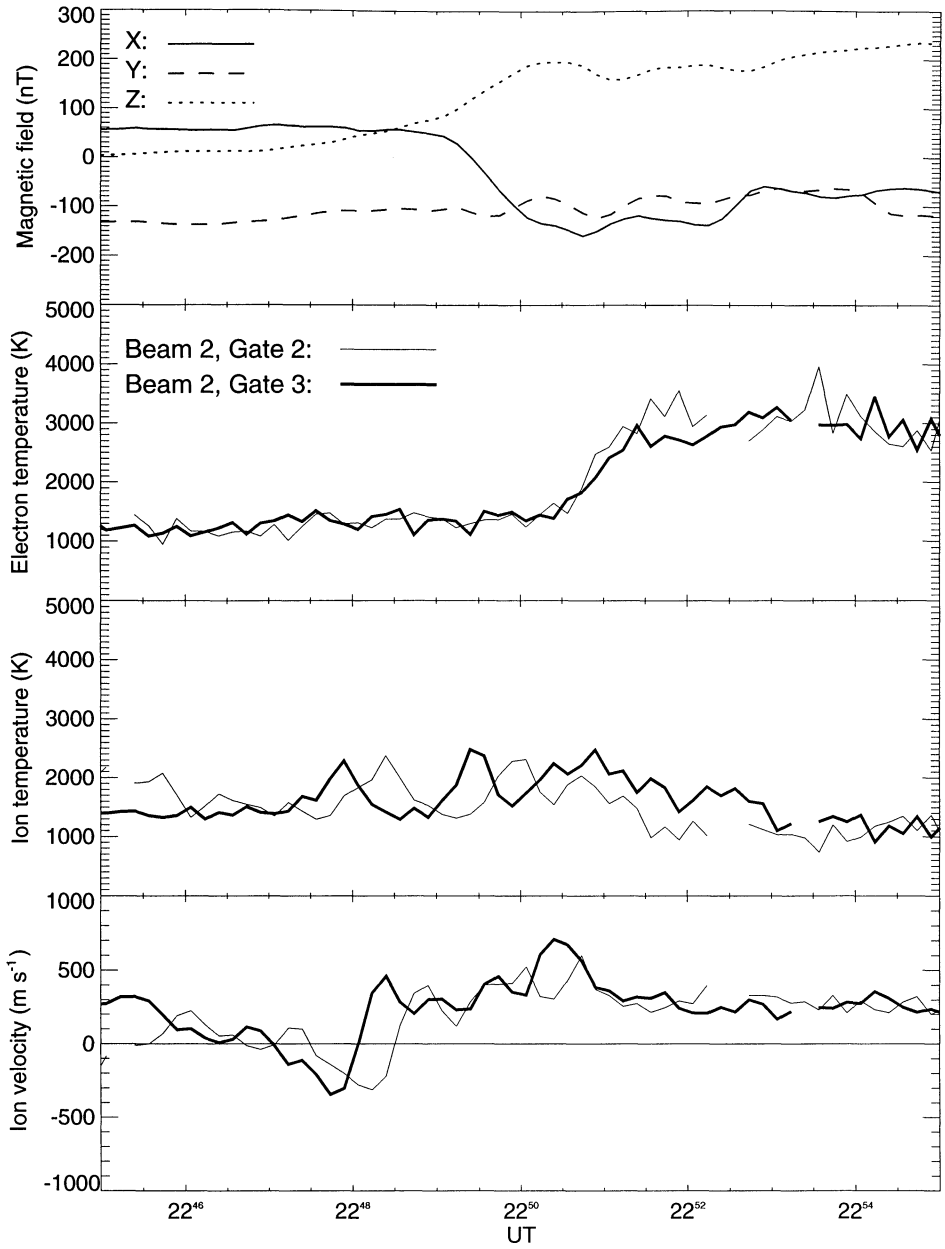

Figure 9. Comparison between magnetic measurements at BJO and radar measurements in gates 2 and 3 of beam 2. The top panel shows the three magnetic components during the interval 2245 to 2255 UT, encompassing the first "spike-like" minimum in the X component. The X component (solid line) is positive toward geographic north, Y (dashed line) is positive toward geographic east, and Z (dotted line) is positive vertically downward. The panels underneath display the radar data for beam 2 gates 2 (thin lines) and 3 (thick lines), showing the electron temperature (second panel), the ion temperature (third panel), and the line-of-sight velocity (bottom panel). The data from gate 2 have been shifted forward in time by 9 s while those from gate 3 have been shifted backward by 21 s, such that the electron temperature passes through 2000 K at ~2250:54 UT, the estimated time that the contour passes overhead at BJO.

BJO, located between gates 2 and 3 of beam 2, where the solid line shows the X component (positive geographic north), the dotted line shows the Y component (positive geographic east), and the dashed line shows the Z component (positive vertically downwards). Assuming that the magnetic effects are due principally to overhead ionospheric Hall currents flowing at an altitude of ~110 km, the equivalent features in the beam plane will then be observed at a point which is connected by the local magnetic field to the point ~110 km vertically above BJO. This point lies almost exactly along the line of beam 2 of the radar (within 0.05° of radar azimuth) at a radar range of 618 km, between gates 2 and 3 (see Figures 1 and 8). From Figure 5 we then infer that the 2000 K T_e boundary passed across the magnetic field line 110 km vertically above BJO 54 s after 2250 UT, compared with 45 s for gate 2 and 75 s for gate 3. In Figure 9 (bottom panels) we have thus shifted

the measurements made in gate 2 of beam 2 (light lines) forward in time by 9 s, and the measurements made in gate 3 (heavy lines) backward in time by 21 s, to form two proxy data sets for a radar gate centered on the field line passing through the E region above BJO. Features associated with the propagating boundary should then line up in these data sets (in particular the 2000 K T_e values should very nearly coincide at 2250:54 UT), while any strictly temporally ordered features will become separated by 30 s (features apparently appearing in gate 3 before gate 2).

If we examine first the magnetic data in the top panel of Figure 9, it can be seen that significant perturbations began at around ~2249:15 UT, when the X component started to decrease and the Z component started to increase, indicating the appearance of the poleward boundary of a sheet eastward overhead current (the Y component perturbations are relatively minor compared with X). The subsequent minimum in the X component (the "spike-like" feature noted in section 2) and the plateauing of the Z component are then seen to coincide very closely with the rise in T_e measured by the radar, confirming that this is due to electron precipitation concurrent with a sharp rise in ionospheric conductivity. The fact that the magnetic deflections began ~100 s before the arrival of the precipitation is taken to be due to the integrating nature of the magnetic observations, as discussed above. The ion temperature enhancement associated with the boundary (not particularly well marked during this interval) coincided with the ~1 min interval during which the electron temperature was increasing, which in turn coincided with the interval encompassing the initial peaks of X and Z. The line-of-sight velocity data show enhanced flows toward the radar in this interval, associated with an inferred enhanced westward flow along the boundary (as in Figure 8a and 8b). The temporal nature of earlier (prebulge) variations in T_i and line-of-sight velocity are also evident in this presentation. These features clearly were not propagating with the poleward moving boundary. In particular, comparison with corresponding data in beam 1 indicates the presence of large ~1 min surges in eastward and equatorward flow centered near 2247 and 2248 UT, as indicated in section 3. It is evident that these flows produced no discernible magnetic effect at BJO, confi ming the low conductivity-of the preboundary ionosphere.

6. Summary

In this paper we have examined ionospheric temperature and velocity data obtained by the EISCAT VHF radar during the poleward propagation of a substorm disturbance over Svalbard in the postmidnight sector, which had been launched by a substorm intensification ~10 min earlier at lower latitudes. It was found that the substorm electrojet region, which propagated poleward at ~1–1.5 km s^{-1}, was associated with a similarly poleward propagating enduring enhancement in the F region electron temperature, from ~1200 to ~3000 K, indicative of soft electron precipitation. The electron temperature boundary was inferred to have a width comparable with or less than one radar range gate (~60 km transverse to the field). A short-lived (~2 min) ion temperature enhancement, from ~1200 to ~2500 K, was also observed, which straddled the rise in electron temperature. This layer extended approximately two gates (~120 km) poleward of the electron temperature boundary and approximately one gate (~60 km) equatorward. It has been shown that the only likely explanation for these elevated ion temperatures is that the ions were heated by elevated plasma flows ~1–2 km s^{-1} within the boundary region, in line with previous theoretical considerations. We note that the timescale of the observed heating and cooling, ~100 s, is much longer than the ion-neutral collision response time, 1–10 s in the F region, such that essentially steady state conditions prevailed within the layer. Detailed analysis of the line-of-sight velocity data in a boundary-aligned coordinate system confirm the presence of rapid flows in the boundary region, peaking at ~1.5–3 km s^{-1}, in cases where the flow conditions on the two beams of the radar experiment appeared to be similar. The direction of the flow can be either westward or eastward along the boundary, depending on the direction of the flow in the poleward region. We infer that this layer of flow is the radar counterpart of the "spike-like" electric fields observed at the poleward boundary of the substorm auroral bulge by *Fujii et al.* [1994], using data from the Dynamics Explorer 2 spacecraft. Noting from the magnetic records that this boundary also contained a sharp jump in ionospheric conductivity, probably by at least an order of magnitude (see the magnetic signature in Figure 9 and corresponding overhead flow), we also infer that this effect is a consequence of the strong jump in conductivity at the boundary, associated with the requirements of magnetosphere-ionosphere flow and current continuity. In effect, the flow in the poleward region tends to be deflected around the high-conductivity boundary, and consequently forms high-speed layers along the boundary in the immediate poleward region.

Acknowledgments. N. J. Fox wishes to acknowledge the support of a National Research Council Award. This work was supported in part by NASA/International Solar Terrestrial Physics Mission grants NAG5-7260 and NAG5-8361. The authors would like to thank the Director of EISCAT and his staff for operating the facility and providing the data. EISCAT is an international association supported by the research councils of Finland (SA), France (CNRS), Germany (MPG), Japan (NIPR), Norway (NAVF), Sweden (NFA), and the United Kingdom (PPARC). J. A. Davies was supported by PPARC grant PPA/G/O/1997/00254. The work was finalized during visits to Leicester by N. J. Fox, supported by PPARC Visiting Fellowship grant PPA/V/O/1997/0025.

Janet G. Luhmann thanks the referees for their assistance in evaluating this paper.

References

Akasofu, S. -I., The development of the auroral substorm, *Planet. Space Sci.*, *12*, 273, 1964.

Davies, J. A., M. Lester, and I. W. McCrea, A statistical study of ion frictional heating observed by EISCAT, *Ann. Geophys.*, *15*, 1399, 1997.

Elphinstone, R. D., and D. J. Hearn, Mapping of the auroral distribution during quiet times and substorm recovery, in *International Conference On Substorms-1*, *Eur. Space Agency Spec. Publ., ESA SP-335*, 13, 1992.

Elphinstone, R. D., J. S. Murphree, D. J. Hearn, W. Heikkila, L. L. Cogger, and I. Sandahl, The auroral distribution and its mapping according to substorm phase, *J. Atmos. Terr. Phys.*, *55*, 1741, 1993.

Fox, N.J., et al., A multipoint study of a substorm occurring on 7 December 1992, and its theoretical implications, *Ann. Geophys.*, *17*, 1369, 1999.

Fujii, R., R. A. Hoffman, P. C. Anderson, J. D. Craven, M. Sugiura, L. A. Frank, and N. C. Maynard, Electrodynamic parameters in the nighttime sector during auroral substorms, *J. Geophys. Res.*, *99*, 6093, 1994.

Fukunishi, H., Y. Takahashi, T. Nagatsuma, T. Mukai, and S. Machida, Latitudinal structures of nightside field-aligned currents and their relationships to the plasma sheet regions, *J. Geophys. Res.*, *98*, 11,235, 1993.

Kelley, M. C., *The Earth's Ionosphere: Plasma Physics and Electrody-*

namics, Academic, San Diego, Calif., 1989.

Lockwood, M., K. Suvanto, J. -P. St. Maurice, K. Kikuchi, B. J. I. Bromage, D. M. Willis, S. R. Crothers, H. Todd, and S. W. H. Cowley, Scattered power from non-thermal, *F*-region plasma observed by EISCAT: Evidence for coherent echoes?, *J. Atmos. Terr. Phys.*, *50*, 467, 1988.

Lockwood, M., I. W. McCrea, G. H. Millward, R. J. Moffett, and H. Rishbeth, EISCAT observations of ion composition and temperature anisotropy in the high-latitude *F*-region, *J. Atmos. Terr. Phys.*, *55*, 895, 1993.

McPherron, R. L., C. T. Russell, and M. Aubry, Satellite studies of magnetospheric substorms on August 15, 1968, 9, Phenomenonological model for substorms, *J. Geophys. Res.*, *78*, 3131, 1973.

Pellinen, R. J., and W. J. Heikkila, Inductive electric fields in the magnetotail and their relation to auroral and substorm phenomena, *Space Sci. Rev.*, *37*, 1, 1984.

Persson, M. A. L., et al., Near-Earth substorm onset: A coordinated study, *Geophys. Res. Lett.*, *21*, 1875, 1994a.

Persson, M. A. L., A. T. Aikio, and H. J. Opgenoorth, Satellite-ground based coordination: Late growth and early expansion phase of a substorm, paper presented at *International Conference on Substorms-2*, University of Alaska, Fairbanks, 157, 1994b.

Raman, R. S. V., J. -P. St. Maurice, and R. S. B. Ong, Incoherent scattering of radar waves in the auroral ionosphere, *J. Geophys. Res.*, *86*, 4751, 1981.

Schunk, R. W., W. J. Raitt, and P. M. Banks, Effects of electric fields on the dayside high-latitude *E*- and *F*-regions, *J. Geophys. Res.*, *80*, 3121, 1975.

St. Maurice, J. -P., and W. B. Hanson, Ion frictional heating at high latitudes and its possible use for an in situ determination of neutral thermospheric winds and temperatures, *J. Geophys. Res.*, *87*, 7580, 1982.

Swartz, W. E., J. F. Providakes, M. C. Kelley, and J. F. Vickrey, The effect of strong velocity shears on incoherent scatter spectra: A new interpretation of unusual high-latitude spectra, *Geophys. Res. Lett.*, *15*, 1341, 1988.

N. J. Fox and R. A. Greenwald, Applied Physics Laboratory, Johns Hopkins University, SRA Group, 11100 Johns Hopkins Rd., Laurel, MD 20723. (nicola.fox@jhuapl.edu)

S. W. H. Cowley, J. A. Davies, and M. Lester, Department of Physics and Astronomy, University of Leicester, Leicester, LE 1 7RH, England.

M. Lockwood, Rutherford Appleton Laboratory, Chilton, Didcot, Oxfordshire OX 11 0QX, England.

H. Lühr, GeoForschungsZentrum Potsdam, Telegrafenberg, D-14473 Potsdam, Germany.

(Received October 15, 1999; revised March 2, 2000;
accepted March 2, 2000.)